

HiRes-LLaVA: Restoring Fragmentation Input in High-Resolution Large Vision-Language Models

Runhui Huang^{1*} Xinpeng Ding^{3*} Chunwei Wang² Jianhua Han²
 Yulong Liu³ Hengshuang Zhao⁴ Hang Xu² Lu Hou² Wei Zhang² Xiaodan Liang^{1†}
¹Shenzhen campus of Sun Yat-sen University ²Huawei
³The Hong Kong University of Science and Technology ⁴The University of Hong Kong

Abstract

High-resolution image inputs allow Large Vision-Language Models (LVLMs) to capture finer visual details, improving comprehension. However, the increased training and computational costs associated with such inputs pose significant challenges. A common approach to mitigate these costs involves slicing the input into uniform patches using sliding windows, each aligned with the vision encoder’s input size. While efficient, this method fragments the input, disrupting the continuity of context, which negatively impacts cross-patch perception tasks. To address these limitations, we propose *HiRes-LLaVA*, a novel framework designed to efficiently process high-resolution inputs of any size without altering the original contextual and geometric information. *HiRes-LLaVA* introduces two key components: (i) a *SliceRestore Adapter (SRA)* that reconstructs sliced patches into their original form, enabling efficient extraction of both global and local features through down-up-sampling and convolutional layers, and (ii) a *Self-Mining Sampler (SMS)* that compresses visual tokens based on internal relationships, preserving original context and positional information while reducing training overhead. To assess the ability of handling context fragmentation, we construct a new benchmark, *EntityGrid-QA*, consisting of edge-related tasks. Extensive experiments demonstrate the superiority of *HiRes-LLaVA* on both existing public benchmarks and *EntityGrid-QA*. For example, with SRA, our method achieves a performance improvement of $\sim 12\%$ over state-of-the-art LVLMs in addressing fragmentation issues. Additionally, our SMS outperforms other visual token downsamplers, while offering high data efficiency.

1. Introduction

Recent progress in Large Vision-Language Models (LVLMs) [2, 38, 40, 41, 52, 84] has significantly en-

*Equal contribution

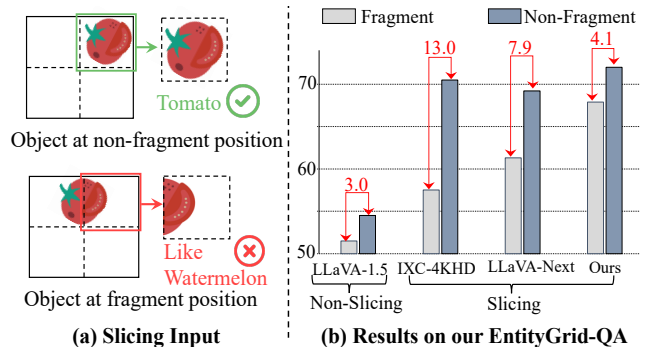


Figure 1. **Illustration of the fragmentation issue.** (a) **Slicing input:** Slicing-based LVLMs, such as LLaVA-Next [53], can fragment objects located at the edges of slices, leading to errors in model understanding. (b) **Performance comparison:** On our EntityGrid-QA benchmark, slicing-based methods show a significant performance gap between fragment and non-fragment inputs. Our method effectively handles both cases, achieving a smaller performance gap similar to non-slicing approaches.

hanced capabilities in vision-language tasks, fostering improved understanding, reasoning, and interaction. Early LVLMs [38, 50, 84] processed images at low resolutions, typically 224×224 , which hindering their ability to capture detailed visual information. This limitation often results in inaccurate recognition of objects and their contextual relationships within images [18, 44].

Enhancing the high-resolution capabilities of LVLMs presents substantial challenges, *i.e.*, training visual encoders to handle high-resolution inputs requires significant computational resources as well as struggling with handling arbitrary image sizes [3, 13]. Recent advances have introduced resource-efficient methods to improve the input resolution of LVLMs. One effective strategy involves using a sliding window technique [23, 44, 55] to segment high-resolution images into smaller patches. These patches are then processed by a visual encoder that has been trained on fixed-size lower-resolution inputs, maintaining computational efficiency while enhancing detail capture.

Slicing-based approaches, while effective, can lead to input fragmentation, as shown in Fig. 1 (a). When objects are located at the edges of slices, the disrupted context can cause misclassifications, such as labeling a ‘Tomato’ as a ‘Watermelon’. This fragmentation compromises spatial relationships and semantic coherence, challenging the model’s understanding. To validate this, we compare non-slicing-based LVLMs, such as LLaVA-1.5 [50], with slicing-based methods like IXC-4KHD [83] and LLaVA-Next [53] under fragmented and non-fragmented scenarios. As shown in Fig. 1 (b), slicing-based methods exhibit a large performance gap (13.0%), while non-slicing-based methods are more consistent (only 3.0% gap), underscoring the limitations of slicing in preserving context integrity. Furthermore, existing methods [23, 55] also rely on Q-Former-like samplers [40] to handle long contexts from high-resolution inputs. However, these samplers suffer from severe drawbacks, such as the lack of positional information and high training overhead [78], making them suboptimal for context-rich scenarios.

In this paper, we propose HiRes-LLaVA, an efficient approach to integrating high-resolution data into LVLMs without disrupting the original context. HiRes-LLaVA introduces the SliceRestore Adapter for the vision encoder to allow the high-resolution slices to preserve the image’s complete context and capture the edge information among slices. This enhancement is processed through dual fusion modules to capture both global and local information in parallel. This lightweight module can be seamlessly integrated into any attention layer of the vision encoder for extracting the features of high-resolution images, enabling efficient fine-tuning without altering pre-trained parameters. Furthermore, HiRes-LLaVA introduces the self-mining sampler that uses pooled sliced patches as queries to compress visual tokens from non-overlapped areas. Unlike fixed learnable query-based methods, our self-mining sampler not only preserves the original context and positional information but also performs high data efficiency.

To evaluate our proposed method, we tested it on nine widely-used public benchmarks and also introduced a new benchmark, EntityGrid-QA, specifically designed to measure how well VLMs handle context fragmentation caused by slicing approaches. Our comprehensive experiments show that HiRes-LLaVA not only performs better than current models on these public benchmarks but also significantly surpasses SOTA LVLMs over 12% on the EntityGrid-QA. Additionally, our SMS outperforms other visual token downsampling methods and improves 40% data efficiency.

2. Related Works

Large vision-language model. Leveraging pre-trained Large Language Models (LLMs) like LLaMA [74] and Vicuna [15], LVLMs have achieved significant advances

in areas such as image/video understanding [2, 9, 39–41, 82, 84], medical analysis [38], and autonomous driving [18, 77]. These models use vision encoders trained via contrastive learning [19, 66] to align visual features with language. Visual embeddings are adapted to match the LLM dimensionality using visual projectors. These projectors can be: (i) resamplers, like Q-Former [2, 40, 84], using fixed queries for cross-attention, or (ii) MLP modules, as seen in the LLaVA series [52]. Recent efforts have aimed to enhance visual representation by combining features from DINO-V2 [65] and SAM [31] with CLIP’s Vision Transformers (ViT) [46, 67]. However, CLIP-ViT’s fixed-resolution requirement (*e.g.*, 336×336) limits the capability to handle higher resolution and varying aspect ratios, thereby hindering performance in fine-grained tasks.

High-resolution large vision-language model. To discern fine-grained visual details from high-resolution inputs, an intuitive approach is to split images into patches and project them using linear layers, treating these as a sequence for input into Large Vision-Language Models (LVLMs) [4, 36]. While this eliminates the need for an image encoder, it often results in insufficient visual representation, leading to increased training costs and suboptimal performance. Alternatively, Up-Resize methods such as Qwen-VL [3] adapt the positional embeddings of ViT from 224×224 to 448×448 and include an additional training phase to fine-tune the ViT. However, this adaptation may alter the original visual position encoding from CLIP-ViT [66], potentially degrading visual representation. Dual-branch approaches introduce a high-resolution branch with lightweight convolutional networks to manage high-resolution inputs but require additional training data and parameters [18, 24, 42, 59]. Slicing-based methods offer a compromise by using slicing windows to divide the high-resolution image into patches that match the input size of a pre-trained vision encoder, maintaining efficiency in parameter use and training data while still achieving competitive performance [23, 44]. However, they suffer from "Context Fragmentation", where the continuity of contextual information across patches is damaged, impacting tasks that require cross-patch context. In this paper, we propose HiRes-LLaVA, a novel technique designed to seamlessly integrate global-local high-resolution details into LVLMs without disrupting the original context, effectively addressing the issue of Context Fragmentation.

3. Method

In this section, we first present the overall framework of HiRes-LLaVA in Sec. 3.1. The two innovative components, namely SliceRestore adapter and self-mining sampler are detailed in Sec. 3.2 and Sec. 3.3 respectively. To further evaluate the ability of VLMs to address the context fragmentation issue, a new benchmark named EntityGrid-QA is proposed in Sec. 3.4.

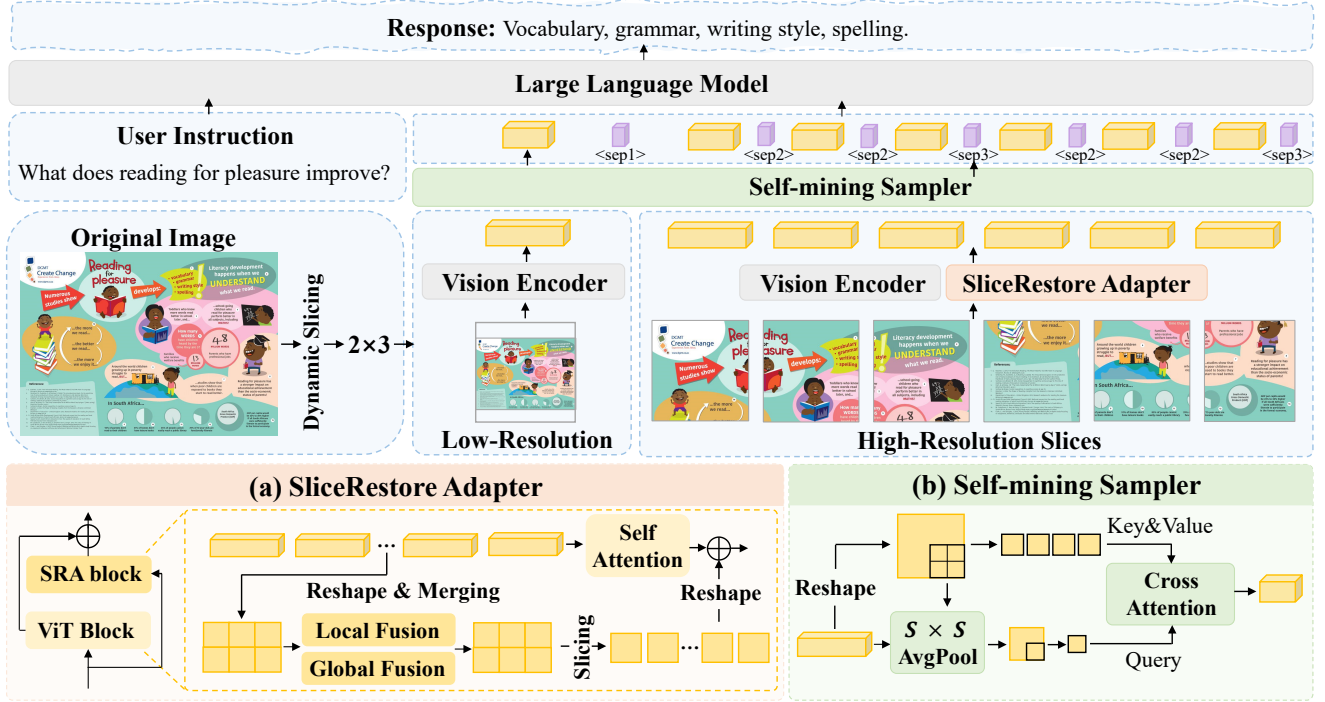


Figure 2. **Overall framework of HiRes-LLaVA.** The vision encoding consists of two branches: one for low-resolution images processed by the pre-trained vision encoder to extract global features, and another dividing high-resolution images into multiple slices to capture fine-grained details. **(a) SliceRestore Adapter** aims to address the Context Fragmentation issue, it restores sliced features into a whole feature by capturing both local and global information, then splits the whole feature back into slices. **(b) Self-Mining Sampler** compresses visual token numbers to reduce computation and memory costs by using downsampled features as queries and the original features as keys and values. Both low-resolution input and each high-resolution slice are compressed by the same self-mining sampler.

3.1. Overall Framework

The overall framework of HiRes-LLaVA is shown in Fig. 2. First, the original image is resized and padded to a low resolution (typically 224×224), then processed by the pre-trained vision encoder to produce global features. To capture fine-grained details, the high-resolution image is split into smaller slices.

Specifically, we set a maximum slice count M , allowing each image to automatically select an optimal slicing grid with m columns and n rows slices. The values of m and n are determined based on the base resolution r of the pretrained vision encoder as follows:

$$m = \left\lceil \frac{H}{r} \right\rceil, \quad n = \left\lceil \frac{W}{r} \right\rceil, \quad (1)$$

This slicing approach adapts to the original aspect ratio of the image. If the resulting number of slices ($4 \times m \times n$) does not exceed the maximum slice count M , the m and n are scale up by a factor of 2, ensuring detailed preservation without overwhelming the model.

After slicing, these slices are processed by a shared vision encoder with the proposed SliceRestore adapter, yielding slice features, followed by a shared self-mining sampler to

reduce token length, resulting in compressed features. Consequently, the visual input to the language model includes a low-resolution overview and multiple high-resolution slices. To maintain clarity, three types of separators are used to maintain clarity in (1) between the low-resolution image and high-resolution slices, (2) between high resolutions slices and (3) the end of each slice row.

3.2. SliceRestore Adapter

We denote the slice features in the l -th layer of ViT as $\{\mathbf{P}_i\}_{i=1}^N$ with $\mathbf{P}_i \in \mathbb{R}^{L \times D}$, where N is the number of slices, $L = H \times W$ is the token length, and D is the feature dimension. Each slice feature is processed individually by the self-attention layer, $Self-Attn(\mathbf{P}_i)$, which lead to a loss of global information in fragmented context. (see Fig. 1 (a)). Although low-resolution inputs contain the overall information, when it comes to real-world scenes, the high-resolution inputs are still needed to perceive the small objects. A naive approach would be concatenating slice features for self-attention, but this incurs quadratic computation costs.

In this paper, we propose the SliceRestore Adapter (SRA) to efficiently capture complete information from high-resolution inputs. As depicted in Fig. 2 (a), the SliceRestore

adapter is integrated into the self-attention layer of vision transformer. This can be formulated as:

$$\{\hat{\mathbf{P}}_i\}_{i=1}^N = \{\mathbf{P}_i\}_{i=1}^N + \{\bar{\mathbf{P}}_i^l\}_{i=1}^N, \quad (2)$$

where:

$$\{\bar{\mathbf{P}}_i^l\}_{i=1}^N = SRA(\{\mathbf{P}_i\}_{i=1}^N), \quad (3)$$

The SliceRestore adapter has three main steps to restore complete semantics from slice features:

1. Merging: Each slice feature \mathbf{P}_i is reshaped to $r \times r \times D$. These reshaped slice features are then merged to recover the original spatial structure, forming the input’s features $\mathbf{F} \in \mathbb{R}^{(m*r) \times (n*r) \times D}$.

2. Capturing: We propose two fusion modules that operate in parallel to capture both local and global context from \mathbf{F} . The local fusion module transfers edge details among slices to facilitate a nuanced exchange of local information. On the other hand, the global fusion module is leveraged to capture broader contextual cues. To achieve this, the local fusion module uses a single layer depth-wise convolution with 3×3 kernel and stride of 1 to efficiently capture local details and retain image-related biases. Due to the high computation cost of self-attention on high-resolution image, the global fusion module employs self-attention on the coarse view of the high-resolution image to transfer the global context to slices. The coarse view image with the same resolution of the low-resolution image, can be simply obtained by downsampling \mathbf{F}^l . After the attention block, the fused global feature is upsampled back to the original size using simple interpolation. The enhanced feature $\bar{\mathbf{F}}$ is obtained by element-wise addition of the outputs from the local and global fusion modules:

$$\bar{\mathbf{F}} = \underbrace{DWConv(\mathbf{F})}_{\text{local fusion}} + \underbrace{Up(Self-Attn(Down(\mathbf{F})))}_{\text{global fusion}}. \quad (4)$$

3. Slicing: Finally, the enhanced feature $\bar{\mathbf{F}}$ is sliced back into the original slice format, resulting in $\{\bar{\mathbf{P}}_i\}_{i=1}^N$, where $\bar{\mathbf{P}}_i \in \mathbb{R}^{L \times D}$.

This process allows model to capture the complete semantics from high-resolution inputs while maintaining computational efficiency.

3.3. Self-Mining Sampler

High-resolution images require processing more visual tokens, significantly increasing the computational load. Existing solutions, such as Q-Former [40], utilize a fixed number of learnable queries to compress visual features through a cross-attention mechanism. While effectively captures visual information regardless of image resolution in a computationally affordable manner, it suffers from several limitations:

(i) Lacking positional information. The learned queries lose positional information, degrading performance in tasks

requiring spatial relationships and precise localization, such as visual reasoning.

(ii) High training overhead. Training Q-Former-like resamplers requires more data and longer training times to convert visual features into learnable queries, posing challenges in data-scarce domains.

To address these issues, we propose the self-mining sampler, as shown in Fig. 2 (b). The key idea of the self-mining sampler is to improve query initialization and reduce the receptive field that each query must compress based on the spatial priors. Specifically, we reshape the 1D output tokens of the vision encoder, (e.g., CLIP-ViT), $\mathbf{P} \in \mathbb{R}^{L \times D}$, into 2D form, $r \times r \times D$, where $L = r \times r$. After applying average-pooling with kernel size $S \times S$, we obtain $\mathbf{P}^c \in \mathbb{R}^{r_2 \times r_2 \times D}$, where $r_2 < r$. Next, we compute the final compressed tokens using the cross-attention mechanism by forcing the compressed token to perceive the $S \times S$ uncompressed tokens. Unlike fixed learnable query-based methods, our self-mining sampler compresses the visual tokens based on themselves, preserving the original context and positional information while reducing training overhead.

3.4. EntityGrid-QA Benchmark

Existing benchmarks, particularly document-related datasets, can evaluate the fine-grained understanding of LVLMs. However, these benchmarks are inadequate for assessing the ability to handle fragmented inputs, as filtering slicing-related questions is time-consuming and labor-intensive. Therefore, we introduce a new benchmark named EntityGrid-QA, which is fully synthesized but still challenging for frontier models, to better assess LVLMs’ ability to handle fragmentation.

Construction process. As shown in Fig. 3, the construction process of EntityGrid-QA consists of three main steps: Entity Sampling, Image Generation, and QA Pairs Generation. Examples of our benchmark are provided in the Appendix. Each step is detailed as follows:

(a) Entity sampling. We first construct an entity set that includes various types such as English Words (e.g., "apple"), Number (e.g., "0.596"), Object (e.g., a teddy bear) and Icon (e.g., "tomato") as shown in Fig. 3 (a). Then, we select several entities from a predefined entity set, which can be denoted as $\mathcal{E} = \{e_i\}_{i=1}^M$, where e_i is the i -th entity and M is the number of selected entities.

(b) Image generation. The selected entities \mathcal{E} are positioned in nine predefined positions (labeled 1 to 9) within a blank image using a 3×3 grid layout, as shown in Fig. 3 (b). The resolution of the blank image is set to $2r \times 2r$, where r is the base resolution of the pretrained vision encoder, e.g., 224×224 . In this way, each image would be divided into four slices, and the each slice would match the input size of well-pretrained vision encoder, without the requirement of additional operations, e.g., resize and padding. Note that our

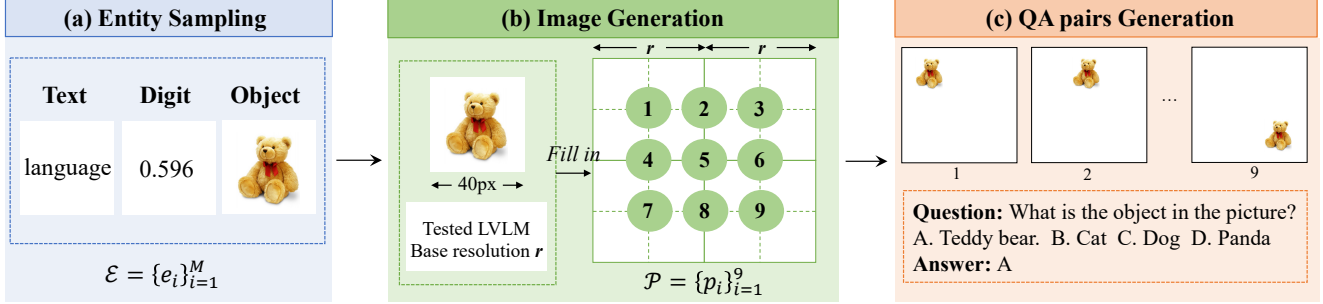


Figure 3. **Construction process of EntityGrid-QA benchmark.** There are three steps: **(a) Entity Sampling.** Select one or two entities from the pre-defined entity set; **(b) Image Generation.** Put the selected entities in one position sampled from the nine pre-defined positions of the blank image, we can obtain the generated images. Note that the dash and solid lines in (b) are for illustration purposes only, and not presented to models. **(c) QA pairs Generation.** Based on the generated images, entity category and positions, we can automatically generate the question-answer pairs (QAs).

HiRes-LLaVA can process any number of slices, but some existing LVLMS, *i.e.*, LLaVA-Next [50] can only receive four slices as input. Hence, for a fair comparison, we only generate the images with a fixed resolution $2r \times 2r$. For each entity e_i , we generate 9 images that iterate over all predefined 9 positions, with each position containing only one entity, as shown in Fig. 3.

(c) QA pairs generation. We mainly focus on evaluating the model’s fine-grained recognition ability on the area of the slice boundary and center of the slices. For each type of entity, we apply a specific question prompt, *e.g.*, "What is the object in the picture?". As shown in Fig. 3 (c), we formulate the question-answer pairs as the multi-choice problem. Based on the selected entity \mathcal{E} and the question Q , we apply the entity-specific augmentation to automatically generate the other three choices for the question. For example, given a number, the optional augmentations can be add, delete or shift the decimal point, or alter one of the digit of the number. Note that for the triplets of image-question-answer of the same entity, it only varies in the position of the generated images while maintaining the same question, order of choices and ground truth answer which is perfectly assess the model.

After the construction, we create a training set of Entity-QA with 2k images covering 4 entity types and a testing set with 720 images and 20 entities per type. The entities in the training set and testing set are non-overlapped. Examples of the benchmark can be found in the Appendix.

Evaluation metric. To evaluate the ability to handle fragmentation, we introduce a new metric that measures the precision discrepancies between entities located at the edge positions ($\mathcal{P}_{\text{edge}} = \{2, 4, 5, 6, 8\}$) and other locations ($\mathcal{P}_{\text{center}} = \{1, 3, 7, 9\}$). We define:

$$Acc_x = \frac{\sum_{p \in \mathcal{P}_x} A_p}{|\mathcal{P}_x|}, \quad x \in \{\text{edge}, \text{center}\} \quad (5)$$

where A_p is the average accuracy when entities are located

at position p , and $|\cdot|$ is the set size.

The Precision Discrepancies (PD) are defined as:

$$PD_1 = \frac{Acc_{\text{edge}}}{Acc_{\text{center}}}, \quad PD_2 = \frac{Acc_{\text{center}} - Acc_{\text{edge}}}{Acc_{\text{center}}} \quad (6)$$

4. Experiment

4.1. Implementation Details

We utilize the CLIP-ViT-L/14-224px [66] and InternViT-300M-448px [14] as the vision encoders, and Vicuna-v1.5-7B [15] and Llama-3.1-Instruction-8B [20] as LLM. We adopt a three-stage training approach, including an alignment stage, a capability enhancement stage and the instruction tuning stage. During the alignment stage, only the self-mining sampler is trainable. The learning rate is $1e-3$. In the capability enhancement stage, we finetune the full model. The learning rate is $2e-5$ for LLM and sampler, and $2e-6$ for ViT. In the instruction tuning stage, ViT is frozen and the SliceRestore adapter is loaded with the LR of $2e-4$. The learning rate of self-mining sampler and LLM is $2e-5$. Four SliceRestore adapters are applied in the last four blocks of the vision encoder. All stages use the batch size of 256.

We adopt AdamW [56] as the optimizer with $\beta_1 = 0.9$ and $\beta_2 = 0.95$ to stabilize the training in the capability enhancement stage and the instruction tuning stage. In all stages, the learning rates are warmed up for the first 0.03 epochs and then adjusted by a cosine scheduler in the remaining training. We don’t apply any weight decay in the training. The maximum number of slices is 9 for InternViT and 16 for CLIP-ViT. Regarding the training data, we use the LLaVA-558k in the alignment stage, 1.8M long caption and OCR data in the capability enhancement stage and 3M multi-tasks data in the instruction tuning stage.

4.2. Experimental Setting

We introduce experimental settings including the benchmarks and the compared LVLMS.

Method	LLM	MaxRes	Document				Science		Comprehensive		
			VQA-text	ChartQA	DocVQA	InfoVQA	SQAI	AI2D	MME	MMB	MM-Vet
<i>General LVLMS (normal resolution)</i>											
Qwen-VL-Chat	Qwen-7B	448x448	61.5	66.3	62.6	-	68.2	57.7	-	60.6	-
LLaVA-1.5	Vicuna-1.5-13B	336x336	61.3	18.2	-	-	71.6	59.5	1826	67.8	36.3
LLaVA-MORE	Llama3.1-Ins-8B	384x384	62.1	-	-	-	77.5	63.6	1846	73.1	-
mPLUG-Owl3	Qwen1.5-7B	384x384	69.0	-	-	-	-	73.4	-	77.6	40.1
<i>Document LVLMS</i>											
DocPedia	Vicuna	2560x2560	60.2	46.9	47.1	15.2	-	-	-	-	-
UReader	Vicuna	896x1120	57.6	59.3	65.4	42.2	-	-	-	-	-
TextMonkey+	Qwen-7B	896x896	64.3	59.9	66.7	28.6	-	-	-	-	-
mPLUG-DocOwl2	Qwen2-7B	1512x2016	66.7	70.0	80.7	<u>46.4</u>	-	-	-	-	-
<i>General LVLMS (higher resolution)</i>											
Monkey	Qwen-7B	896x896	67.6	-	66.5	36.1	-	-	-	-	-
LLaVA-NeXT-8B	LLama3-Ins-8b	672x672	64.6	69.5	72.6	-	-	71.6	1603/-	72.1	41.7
LLaVA-NeXT-13B	Vicuna-13B	672x672	67.1	62.2	70.9	-	73.6	70.0	1901	70.0	<u>48.4</u>
LLaVA-UHD	Vicuna-13B	672x1008	67.7	-	-	-	72.0	-	1535/-	68.0	-
Mini-Gemini-HD	Llama3-Ins-8b	672x672	70.2	59.1	74.6	-	75.1	73.5	1606/-	72.7	-
Cambrian-1-8B	Llama3-Ins-8B	1024x1024	71.7	73.3	77.8	-	<u>80.4</u>	73.0	1547/-	<u>75.9</u>	-
Cambrian-1-13B	Vicuna-1.5-13B	1024x1024	<u>72.8</u>	<u>73.8</u>	76.8	-	79.3	<u>73.6</u>	1610/-	75.7	-
HiRes-LLaVA	Llama3.1-Ins-8B	1344x1344	74.2	77.4	84.9	55.7	90.3	74.9	2213	75.7	53.5

Table 1. **Quantitative results on 9 popular benchmarks.** ‘MaxRes’ means the maximum resolution supported. ‘Document’, ‘Science’ and ‘Comprehensive’ indicate the document-related VQA, Science VQA and comprehensive benchmarks.

Model	$Acc_{mean} \uparrow$	$Acc_{std} \downarrow$	$Acc_e \uparrow$	$Acc_c \uparrow$	$PD_1 \uparrow$	$PD_2 \downarrow$
LLaVA-1.5	53.33	0.19	52.00	55.00	94.50	5.45
LLaVA-NeXT	65.22	0.30	61.80	69.50	88.92	11.07
IXC-4KHD	63.78	0.53	58.00	71.00	81.69	18.31
HiRes-LLaVA	70.20	0.19	68.40	72.50	94.34	5.60

Table 2. **Comparison with the state-of-the-art methods on EntityGrid-QA.** ‘ \downarrow ’ indicates lower scores are better, while ‘ \uparrow ’ means the opposite. ‘ Acc_{mean} ’ and ‘ Acc_{std} ’, representing the mean and standard deviation of the average accuracy across three tasks. ‘ Acc_e ’ and ‘ Acc_c ’ show the average accuracy for entities at \mathcal{P}_{edge} and \mathcal{P}_{center} , respectively. PD_1 and PD_2 are calculated using Eq. (6). Note that IXC-4KHD and HiRes-LLaVA are evaluated on 896x896 images and LLaVA-NeXT is evaluated on 672x672 images. The input resolution for LLaVA is 336px.

Benchmarks. We evaluate our models on (i) document-oriented VQA benchmarks, including VQA-Text [69], ChartQA test set [60], DocVQA test set [61], InfoVQA test set [62]; (ii) general VQA benchmarks, including AI2D [28], ScienceQA [58]; (iii) comprehensive benchmarks, including MMBench [54], MME [22] and MM-Vet [81].

Compared LVLMS. We compare our model with SOTA LVLMS. (1) General LVLMS, *i.e.*, Qwen-VL [3], LLaVA-1.5 [50], LLaVA-MORE [17], mPLUG-Owl3 [79], Monkey [44], Mini-Gemini [43], LLaVA-UHD [23], LLaVA-NeXT [53] and Cambrian-1 [73]. (2) Document LVLMS, *i.e.*, DocPedia [21], UReader [80], TextMonkey [55] and mPLUG-Docowl2 [25].

4.3. State-of-the-art Comparison

General benchmarks. Table 1 reports the performance comparison of our methods against state-of-the-art approaches on 11 benchmarks. Specifically, HiRes-LLaVA surpasses those general LVLMS with normal resolution inputs. As for the document LVLMS with higher resolution inputs, HiRes-LLaVA demonstrates better performance on those document-related VQA benchmarks, for example, achieving 74.2 vs 66.7 of mPLUG-DocOwl2 on VQA-text, proving its capability to manage document-related tasks effectively. Compared to Cambrian-1-13B that employs 4 vision encoders and is trained on 7M SFT data, our HiRes-LLaVA, with 8B LLM, one vision encoder and trained on 50% less data than Cambrian-1, achieves better performance. These results indicate that HiRes-LLaVA has stronger generalization ability and robustness when dealing with complex documents, scientific problems, and comprehensive challenges.

Figure 4 shows a visual comparison of results generated by LLaVA-NeXT [50], Monkey [44], and our method, highlighting our superior performance, especially when the region of interest spans across slices. For example, the number 1.14 in Fig. 4 (b) is split into two slices, causing Monkey to misidentify it as 1.4.

Our method, with the SRA capturing complete global high-resolution information, correctly predicts the answers. **EntityGrid-QA.** To evaluate the ability to address input fragmentation, we compare LLaVA-1.5 with normal res-

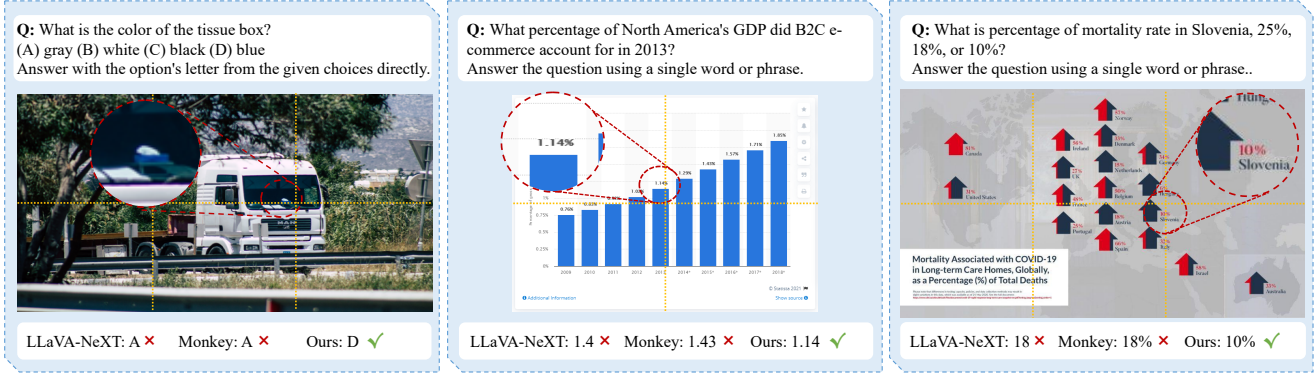


Figure 4. Visualization comparison with the state-of-the-art methods. Dash lines are only illustrated for the slice clarify.

Components			Document					Comprehensive		
Downsampler	SRA	Separator	VQA-Text	ChartQA	DocQA	InfoVQA	Avg.	MMB	MM-Vet	MME-P
Baseline(LLaVA)			53.3	23.8	22.6	26.0	31.4	64.0	-	1424.7
ConcatChannel	✗	✗	60.3	54.4	54.8	34.3	50.9	60.8	30.2	1355.5
Resampler	✗	✗	58.8	49.8	42.8	32.6	46.0	59.6	26.6	1404.0
C-Abstractor	✗	✗	59.0	55.6	54.7	36.7	51.5	63.5	30.4	1393.5
SMS	✗	✗	60.0	56.2	58.0	37.4	52.9	63.3	31.1	1411.3
SMS	G	✗	60.9	56.2	57.2	38.2	53.1	65.5	30.6	1415.8
SMS	G & L	✗	61.5	56.9	57.6	38.4	53.6	64.9	33.8	1452.9
SMS	G & L	✓	61.8	58.8	59.7	41.4	55.4	65.5	33.8	1456.1
improvement relative to the baseline			+8.5	+35.0	+37.1	+15.4	+24.0	+1.5	-	+31.4

Table 3. Ablation study of different proposed modules. Note that ‘G’, and ‘G-L’ indicate using the global fusion and the combination of them respectively. All results are conducted with the maximum number of slices is 16 except the baseline model, LLaVA. The last row is the improvement over the baseline model.

olution input and two SOTA slicing-based LVLMS. The results are presented in Tab. 2. According to the experimental results, we can observe two key findings: (i) Slicing the high-resolution image will bring the fragmentation issue. Although LLaVA-NeXT performs better than LLaVA-1.5 on both Acc_e and Acc_c , it suffers significantly from fragmentation, as indicated by a 5.58% drop in PD_1 and a 5.62% increase in PD_2 . (ii) Our method, utilizing SRA, significantly outperforms SOTA LVLMS in handling entities at the edges of slices. For example, IXC-4KHD (InternLM-Xcomposer-4KHD)[83] exhibits a notable discrepancy between Acc_e and Acc_c , with scores of 58.0% and 71.0%, respectively. In contrast, our method achieves higher accuracy at both the edges and the center of the slices (68.4% for Acc_e and 72.5% for Acc_c) and also obtains a smaller difference, with 94.34% for PD_1 and 5.6% for PD_2 , which is close to the LVLMS with normal resolution inputs.

4.4. Ablation Study

In this section, we conduct ablation studies to evaluate the effect of our proposed modules. In our ablation study, we conduct the experiments following LLaVA’s setting on the LLaVA 1.2M data [50] with additional 79K document-oriented data, which is essential to evaluate the

M	#Tokens	VQA-Text	ChartQA	DocQA	InfoVQA	MMB	MME-P
4	~320	56.2	42.5	37.0	28.8	65.1	1436.3
9	~640	59.9	51.6	49.3	34.9	64.3	1450.0
16	~1088	61.8	58.8	59.7	41.4	65.5	1456.1

Table 4. Effect of different numbers of slices. M and ‘#Tokens’ indicate the maximum number of slices and visual tokens in the high-resolution images, respectively.

high-resolution LVLMS, in the instruction tuning stage, i.e., DocVQA [61], ChartQA [60] and InfoVQA [62]. Unless specified, we use LoRA [26] to efficiently finetune pretrained LLM, i.e., Vicuna-1.5-7B and CLIP-ViT-Large-224px as the vision encoder with maximum 16 slices in our ablation.

Effect of the proposed modules. We ablate the two main components of our HiRes-LLaVA, specifically the SliceRestore adapter (SRA) and the self-mining sampler (SMS), as shown in Tab. 3. Our findings are as follows: Our SMS demonstrates superior performance compared to other samplers, notably outperforming Resampler [3] by 6.9% on the average score across four benchmarks. Integrating the model with SRA leads to further improvements across these benchmarks. Additionally, the introduction of learnable queries to isolate slice representations, referred to as Separator, results in a 1.8% enhancement in the average score.

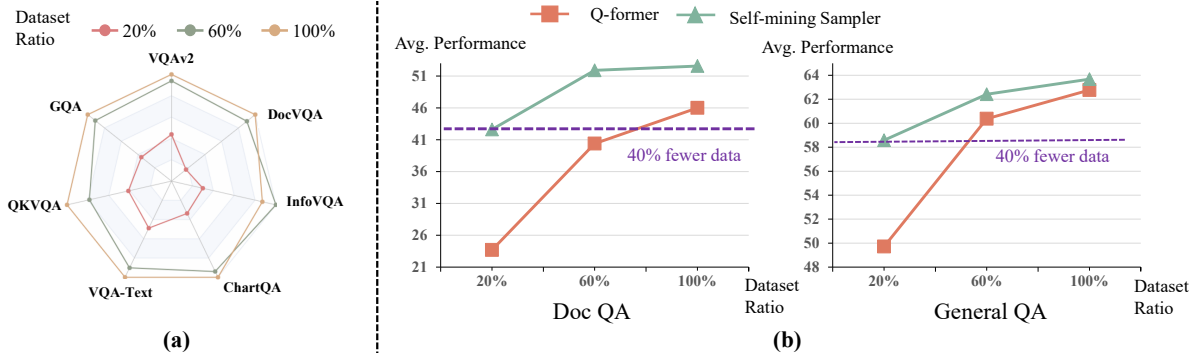


Figure 5. (a) **Ablation on data efficiency of HiRes-LLaVA.** We sample the training data mixture at ratios of 20%, 60%, and 100% and report the performance of our HiRes-LLaVA on seven benchmarks. (b) **Data efficiency comparison with Q-former and our proposed self-mining sampler (SMS).** The performance on ‘Doc QA’ is averaged from DocVQA, ChartQA and InfoVQA. The performance on ‘General QA’ is averaged from the other four benchmarks. Our SMS can use 40% fewer data to achieve competitive performance compared with Q-former, indicating our method’s efficiency. Note that both Q-former and our SMS apply one cross-attention block.

Base Res.	Kernel Size	Max #Tokens (Token/Slice)	VQA-Text	ChartQA	DocVQA	InfoVQA	Avg.
224	2 × 2	1088 (64)	61.8	58.8	59.7	41.4	55.4
224	4 × 4	272 (16)	59.6	53.9	46.3	33.0	48.2
224	8 × 8	68 (4)	54.9	46.8	35.3	29.6	41.7
336	2 × 2	2448 (144)	63.6	58.5	65.7	40.7	57.1
336	3 × 3	1088 (64)	61.2	56.7	59.8	38.7	54.1
336	4 × 4	512 (36)	61.4	53.3	54.3	34.3	50.8

Table 5. **Effect of different downsample kernel sizes in the self-mining sampler.** ‘Kernel Size’ is $S \times S$ defined in Sec. 3.3. ‘Base Res.’ indicates the base resolution of the vision encoder. ‘Max #Tokens’ indicates the maximum number of visual tokens, *i.e.*, $M \times r_2 \times r_2$, as the maximum number of slices M is 16.

Ablation study of kernel sizes in SMS. Here we conduct the ablation study of the self-mining sampler. In Tab. 5, we compare the performance of the average pooling with different kernel sizes, *i.e.*, $S \times S$ in Sec. 3.3. The results show that as the kernel size increases, *i.e.*, the fewer visual tokens, the performance would degrade, since the information loss.

Ablation study of the number of high-resolution image slices. As shown in Tab. 4, the number of slices significantly affects the model’s performance on the document-related benchmarks. Specifically, when increasing the number of slices from 4 to 16, the average performance improves by 14.3% on four document-related benchmarks. As for the comprehensive benchmarks, larger number of slices doesn’t effect model’s performance on MMBench too much and can bring a 19.8 improvement on MME-Perception.

Ablation study of the selection of vision encoder and language model. In Tab. 6, we evaluate the performance of different vision encoders and large language models on LVLMBenchmarks. Experimental results show that compared to Vicuna-1.5-7B, LLaMA3.1-8B-Instruct can significantly improve the model’s performance on both document-related benchmarks and comprehensive benchmarks. Additionally, InternViT-300M-448px can maintain performance on com-

Vision Encoder	LLM	VQA-Text	ChartQA	DocQA	InfoVQA	MMB	MME-P
CLIP-ViT-224px	Vicuna	61.8	58.8	59.7	41.4	65.5	1456.1
CLIP-ViT-224px	Llama3.1	60.5	58.6	67.2	47.2	68.1	1453.4
InternViT-448px	Llama3.1	63.4	65.9	74.4	53.2	68.0	1459.1

Table 6. **The ablation study of different vision encoder and large language models.** Note that CLIP-ViT-224px uses 16 maximum slices and InternViT-448px uses 9 slices.

prehensive benchmarks and further improve all document-related benchmarks by increasing the base resolution and the number of visual tokens.

Data efficiency analysis. We evaluated the data efficiency of our method, HiRes-LLaVA, by subsampling the training data mixture at ratios of 20%, 60%, and 100%. Results in Fig. 5 (a) show that using the entire dataset achieves optimal performance. Remarkably, with only 60% of the data, performance remains above 90% of the full dataset’s level, highlighting the potential for improved data efficiency. Additionally, we compared our self-mining sampler’s efficiency against the commonly used Q-former in LVLMs. As depicted in Fig. 5 (b), our method performs competitively with Q-former even with only 20% of the data, demonstrating its effectiveness and efficiency.

5. Conclusion

In this paper, we present HiRes-LLaVA, a large visual-language model (LVLMB) designed to efficiently address input fragmentation caused by current slicing-based high-resolution LVLMBs. To evaluate this capability, we introduce a new benchmark, EntityGrid-QA, which focused on identification tasks on various entities. Comprehensive experimental results on 9 popular existing benchmarks and EntityGrid-QA demonstrate the effectiveness of HiRes-LLaVA. Analytical evaluation and visualization results are provided for a deeper understanding of the model’s performance.

Acknowledgements

We gratefully acknowledge supports of MindSpore, CANN (Compute Architecture for Neural Networks) and Ascend AI Processor used for this research. This work is supported by National Key Research and Development Program of China (2024YFE0203100), Shenzhen Science and Technology Program No.GJHZ20220913142600001, National Natural Science Foundation of China (NSFC) (No.62476293, 62441615 and 62201484), Nansha Key R&D Program under Grant No.2022ZD014 and General Embodied AI Center of Sun Yat-sen University.

References

- [1] 100TAL. TAL Education Group. <https://ai.100tal.com/dataset>, 2023. 13
- [2] Jean-Baptiste Alayrac, Jeff Donahue, Pauline Luc, Antoine Miech, Iain Barr, Yana Hasson, Karel Lenc, Arthur Mensch, Katherine Millican, Malcolm Reynolds, et al. Flamingo: a visual language model for few-shot learning. *Advances in Neural Information Processing Systems*, 35:23716–23736, 2022. 1, 2
- [3] Jinze Bai, Shuai Bai, Shusheng Yang, Shijie Wang, Sinan Tan, Peng Wang, Junyang Lin, Chang Zhou, and Jingren Zhou. Qwen-vl: A versatile vision-language model for understanding, localization, text reading, and beyond. *arXiv preprint arXiv:2308.12966*, 2023. 1, 2, 6, 7, 15
- [4] Rohan Bavishi, Erich Elsen, Curtis Hawthorne, Maxwell Nye, Augustus Odena, Arushi Somani, and Saġnak Taşlılar. Introducing our multimodal models, 2023. 2
- [5] Ali Furkan Biten, Ruben Tito, Andres Mafla, Lluís Gomez, Marçal Rusinol, Ernest Valveny, CV Jawahar, and Dimosthenis Karatzas. Scene text visual question answering. In *ICCV*, pages 4291–4301, 2019. 13
- [6] Junbum Cha, Wooyoung Kang, Jonghwan Mun, and Byungseok Roh. Honeybee: Locality-enhanced projector for multimodal llm. In *Proceedings of the IEEE/CVF Conference on Computer Vision and Pattern Recognition (CVPR)*, 2024. 15
- [7] Guiming Hardy Chen, Shunian Chen, Ruifei Zhang, Junying Chen, Xiangbo Wu, Zhiyi Zhang, Zhihong Chen, Jianquan Li, Xiang Wan, and Benyou Wang. Allava: Harnessing gpt4v-synthesized data for a lite vision-language model, 2024. 13
- [8] Jun Chen, Deyao Zhu, Xiaoqian Shen, Xiang Li, Zechun Liu, Pengchuan Zhang, Raghuraman Krishnamoorthi, Vikas Chandra, Yunyang Xiong, and Mohamed Elhoseiny. Minigt-v2: Large language model as a unified interface for vision-language multi-task learning. *arXiv:2310.09478*, 2023. 15
- [9] Keqin Chen, Zhao Zhang, Weili Zeng, Richong Zhang, Feng Zhu, and Rui Zhao. Shikra: Unleashing multimodal llm’s referential dialogue magic. *arXiv preprint arXiv:2306.15195*, 2023. 2
- [10] Lin Chen, Jinsong Li, Xiaoyi Dong, Pan Zhang, Conghui He, Jiaqi Wang, Feng Zhao, and Dahua Lin. Sharegpt4v: Improving large multi-modal models with better captions. In *European Conference on Computer Vision*, pages 370–387. Springer, 2024. 13
- [11] Wenhui Chen, Hongmin Wang, Jianshu Chen, Yunkai Zhang, Hong Wang, Shiyang Li, Xiyou Zhou, and William Yang Wang. Tabfact: A large-scale dataset for table-based fact verification. *arXiv preprint arXiv:1909.02164*, 2019. 13
- [12] Xingyu Chen, Zihan Zhao, Lu Chen, Jiabao Ji, Danyang Zhang, Ao Luo, Yuxuan Xiong, and Kai Yu. Websrc: A dataset for web-based structural reading comprehension. In *Proceedings of the 2021 Conference on Empirical Methods in Natural Language Processing*, pages 4173–4185, 2021. 13
- [13] Xi Chen, Xiao Wang, Lucas Beyer, Alexander Kolesnikov, Jialin Wu, Paul Voigtlaender, Basil Mustafa, Sebastian Goodman, Ibrahim Alabdulmohsin, Piotr Padlewski, et al. Pali-3 vision language models: Smaller, faster, stronger. *arXiv preprint arXiv:2310.09199*, 2023. 1
- [14] Zhe Chen, Jiannan Wu, Wenhui Wang, Weijie Su, Guo Chen, Sen Xing, Zhong Muyan, Qinglong Zhang, Xizhou Zhu, Lewei Lu, et al. Internvl: Scaling up vision foundation models and aligning for generic visual-linguistic tasks. *arXiv preprint arXiv:2312.14238*, 2023. 5
- [15] Wei-Lin Chiang, Zhuohan Li, Zi Lin, Ying Sheng, Zhanghao Wu, Hao Zhang, Lianmin Zheng, Siyuan Zhuang, Yonghao Zhuang, Joseph E Gonzalez, et al. Vicuna: An open-source chatbot impressing gpt-4 with 90%* chatgpt quality. See <https://vicuna.lmsys.org> (accessed 14 April 2023), 2023. 2, 5
- [16] Christopher Clark and Matt Gardner. Simple and effective multi-paragraph reading comprehension. In *ACL*, pages 845–855, 2018. 13
- [17] Federico Cocchi, Nicholas Moratelli, Davide Caffagni, Sara Sarto, Marcella Cornia, Lorenzo Baraldi, and Rita Cucchiara. LLaVA-MORE: Enhancing Visual Instruction Tuning with LLaMA 3.1, 2024. 6
- [18] Xinpeng Ding, Jianhua Han, Hang Xu, Wei Zhang, and Xiaomeng Li. Hilm-d: Towards high-resolution understanding in multimodal large language models for autonomous driving. *arXiv preprint arXiv:2309.05186*, 2023. 1, 2
- [19] Alexey Dosovitskiy, Lucas Beyer, Alexander Kolesnikov, Dirk Weissenborn, Xiaohua Zhai, Thomas Unterthiner, Mostafa Dehghani, Matthias Minderer, Georg Heigold, Sylvain Gelly, et al. An image is worth 16x16 words: Transformers for image recognition at scale. *arXiv preprint arXiv:2010.11929*, 2020. 2
- [20] Abhimanyu Dubey, Abhinav Jauhri, Abhinav Pandey, Abhishek Kadian, Ahmad Al-Dahle, Aiesha Letman, Akhil Mathur, Alan Schelten, Amy Yang, Angela Fan, et al. The Llama 3 herd of models. *arXiv preprint arXiv:2407.21783*, 2024. 5
- [21] Hao Feng, Qi Liu, Hao Liu, Wengang Zhou, Houqiang Li, and Can Huang. Docpedia: Unleashing the power of large multimodal model in the frequency domain for versatile document understanding. *arXiv preprint arXiv:2311.11810*, 2023. 6
- [22] Chaoyou Fu, Peixian Chen, Yunhang Shen, Yulei Qin, Mengdan Zhang, Xu Lin, Zhenyu Qiu, Wei Lin, Jinrui Yang, Xiawu Zheng, et al. Mme: A comprehensive evaluation benchmark for multimodal large language models. *arXiv preprint arXiv:2306.13394*, 2023. 6

- [23] Zonghao Guo, Ruyi Xu, Yuan Yao, Junbo Cui, Zanlin Ni, Chunjiang Ge, Tat-Seng Chua, Zhiyuan Liu, and Gao Huang. Llava-uhd: an lmm perceiving any aspect ratio and high-resolution images. In *European Conference on Computer Vision*, pages 390–406. Springer, 2024. 1, 2, 6, 15
- [24] Wenyi Hong, Weihang Wang, Qingsong Lv, Jiazheng Xu, Wenmeng Yu, Junhui Ji, Yan Wang, Zihan Wang, Yuxiao Dong, Ming Ding, and Jie Tang. Cogagent: A visual language model for gui agents, 2023. 2
- [25] Anwen Hu, Haiyang Xu, Liang Zhang, Jiabo Ye, Ming Yan, Ji Zhang, Qin Jin, Fei Huang, and Jingren Zhou. mplug-docowl2: High-resolution compressing for ocr-free multi-page document understanding. *arXiv preprint arXiv:2409.03420*, 2024. 6
- [26] Edward J Hu, Yelong Shen, Phillip Wallis, Zeyuan Allen-Zhu, Yuanzhi Li, Shean Wang, Lu Wang, and Weizhu Chen. Lora: Low-rank adaptation of large language models. *arXiv preprint arXiv:2106.09685*, 2021. 7
- [27] Kushal Kafle, Brian Price, Scott Cohen, and Christopher Kanan. Dvqa: Understanding data visualizations via question answering. In *CVPR*, pages 5648–5656, 2018. 13
- [28] Aniruddha Kembhavi, Mike Salvato, Eric Kolve, Minjoon Seo, Hannaneh Hajishirzi, and Ali Farhadi. A diagram is worth a dozen images. In *ECCV*, pages 235–251, 2016. 6, 13
- [29] Aniruddha Kembhavi, Minjoon Seo, Dustin Schwenk, Jonghyun Choi, Ali Farhadi, and Hannaneh Hajishirzi. Are you smarter than a sixth grader? textbook question answering for multimodal machine comprehension. In *CVPR*, pages 4999–5007, 2017. 13
- [30] Geewook Kim, Teakgyu Hong, Moonbin Yim, JeongYeon Nam, Jinyoung Park, Jinyeong Yim, Wonseok Hwang, Sangdoon Yun, Dongyoon Han, and Seunghyun Park. Ocr-free document understanding transformer. In *ECCV*, 2022. 13
- [31] Alexander Kirillov, Eric Mintun, Nikhila Ravi, Hanzi Mao, Chloe Rolland, Laura Gustafson, Tete Xiao, Spencer Whitehead, Alexander C. Berg, Wan-Yen Lo, Piotr Dollár, and Ross Girshick. Segment anything. *arXiv:2304.02643*, 2023. 2
- [32] Shanghai AI Laboratory. Sharegpt-4o: Comprehensive multi-modal annotations with gpt-4o, 2023. 13
- [33] LAION. Gpt-4v dataset. <https://huggingface.co/datasets/laion/gpt4v-dataset>, 2023. 13
- [34] Hugo Laurençon, Léo Tronchon, Matthieu Cord, and Victor Sanh. What matters when building vision-language models?, 2024. 13
- [35] Paul Lerner, Olivier Ferret, Camille Guinaudeau, Hervé Le Borgne, Romaric Besançon, José G Moreno, and Jesús Lovón Melgarejo. Viquae, a dataset for knowledge-based visual question answering about named entities. In *SIGIR*, pages 3108–3120, 2022. 13
- [36] Bo Li, Peiyuan Zhang, Jingkang Yang, Yuanhan Zhang, Fanyi Pu, and Ziwei Liu. Otterhd: A high-resolution multi-modality model. *arXiv preprint arXiv:2311.04219*, 2023. 2
- [37] Bo Li*, Peiyuan Zhang*, Kaichen Zhang*, Fanyi Pu*, Xinrun Du, Yuhao Dong, Haotian Liu, Yuanhan Zhang, Ge Zhang, Chunyuan Li, and Ziwei Liu. Lmms-eval: Accelerating the development of large multimodal models, 2024. 13
- [38] Chunyuan Li, Cliff Wong, Sheng Zhang, Naoto Usuyama, Haotian Liu, Jianwei Yang, Tristan Naumann, Hoifung Poon, and Jianfeng Gao. Llava-med: Training a large language-and-vision assistant for biomedicine in one day. *arXiv preprint arXiv:2306.00890*, 2023. 1, 2, 13
- [39] Junnan Li, Dongxu Li, Caiming Xiong, and Steven Hoi. Blip: Bootstrapping language-image pre-training for unified vision-language understanding and generation. In *International Conference on Machine Learning*, pages 12888–12900. PMLR, 2022. 2
- [40] Junnan Li, Dongxu Li, Silvio Savarese, and Steven Hoi. Blip-2: Bootstrapping language-image pre-training with frozen image encoders and large language models. *arXiv preprint arXiv:2301.12597*, 2023. 1, 2, 4
- [41] KunChang Li, Yanan He, Yi Wang, Yizhuo Li, Wenhai Wang, Ping Luo, Yali Wang, Limin Wang, and Yu Qiao. Videochat: Chat-centric video understanding. *arXiv preprint arXiv:2305.06355*, 2023. 1, 2
- [42] Yanwei Li, Yuechen Zhang, Chengyao Wang, Zhisheng Zhong, Yixin Chen, Ruihang Chu, Shaoteng Liu, and Jiaya Jia. Mini-gemini: Mining the potential of multi-modality vision language models. *arXiv preprint arXiv:2403.18814*, 2024. 2
- [43] Yanwei Li, Yuechen Zhang, Chengyao Wang, Zhisheng Zhong, Yixin Chen, Ruihang Chu, Shaoteng Liu, and Jiaya Jia. Mini-gemini: Mining the potential of multi-modality vision language models. *arXiv preprint arXiv:2403.18814*, 2024. 6
- [44] Zhang Li, Biao Yang, Qiang Liu, Zhiyin Ma, Shuo Zhang, Jingxu Yang, Yabo Sun, Yuliang Liu, and Xiang Bai. Monkey: Image resolution and text label are important things for large multi-modal models. *arXiv preprint arXiv:2311.06607*, 2023. 1, 2, 6
- [45] Tsung-Yi Lin, Michael Maire, Serge Belongie, James Hays, Pietro Perona, Deva Ramanan, Piotr Dollár, and C Lawrence Zitnick. Microsoft coco: Common objects in context. In *ECCV*, pages 740–755, 2014. 13
- [46] Ziyi Lin, Chris Liu, Renrui Zhang, Peng Gao, Longtian Qiu, Han Xiao, Han Qiu, Chen Lin, Wenqi Shao, Keqin Chen, Jiaming Han, Siyuan Huang, Yichi Zhang, Xuming He, Hongsheng Li, and Yu Qiao. Sphinx: The joint mixing of weights, tasks, and visual embeddings for multi-modal large language models. 2
- [47] Fangyu Liu, Guy Emerson, and Nigel Collier. Visual spatial reasoning. *ACL*, 11:635–651, 2023. 13
- [48] Fuxiao Liu, Kevin Lin, Linjie Li, Jianfeng Wang, Yaser Yacoob, and Lijuan Wang. Aligning large multi-modal model with robust instruction tuning. *arXiv preprint arXiv:2306.14565*, 2023. 13
- [49] Fuxiao Liu, Xiaoyang Wang, Wenlin Yao, Jianshu Chen, Kaiqiang Song, Sangwoo Cho, Yaser Yacoob, and Dong Yu. Mmc: Advancing multimodal chart understanding with large-scale instruction tuning. *arXiv preprint arXiv:2311.10774*, 2023. 13
- [50] Haotian Liu, Chunyuan Li, Yuheng Li, and Yong Jae Lee. Improved baselines with visual instruction tuning. *arXiv preprint arXiv:2310.03744*, 2023. 1, 2, 5, 6, 7

- [51] Haotian Liu, Chunyuan Li, Qingyang Wu, and Yong Jae Lee. Visual instruction tuning. *NeurIPS*, 36, 2023. 13
- [52] Haotian Liu, Chunyuan Li, Qingyang Wu, and Yong Jae Lee. Visual instruction tuning. *arXiv preprint arXiv:2304.08485*, 2023. 1, 2
- [53] Haotian Liu, Chunyuan Li, Yuheng Li, Bo Li, Yuanhan Zhang, Sheng Shen, and Yong Jae Lee. Llava-next: Improved reasoning, ocr, and world knowledge, 2024. 1, 2, 6, 13
- [54] Yuan Liu, Haodong Duan, Yuanhan Zhang, Bo Li, Songyang Zhang, Wangbo Zhao, Yike Yuan, Jiaqi Wang, Conghui He, Ziwei Liu, et al. Mmbench: Is your multi-modal model an all-around player? *arXiv preprint arXiv:2307.06281*, 2023. 6
- [55] Yuliang Liu, Biao Yang, Qiang Liu, Zhang Li, Zhiyin Ma, Shuo Zhang, and Xiang Bai. Textmonkey: An ocr-free large multimodal model for understanding document. *arXiv preprint arXiv:2403.04473*, 2024. 1, 2, 6
- [56] Ilya Loshchilov and Frank Hutter. Decoupled weight decay regularization. In *International Conference on Learning Representations*. 5
- [57] Pan Lu, Liang Qiu, Jiaqi Chen, Tony Xia, Yizhou Zhao, Wei Zhang, Zhou Yu, Xiaodan Liang, and Song-Chun Zhu. Iconqa: A new benchmark for abstract diagram understanding and visual language reasoning. *arXiv preprint arXiv:2110.13214*, 2021. 13
- [58] Pan Lu, Swaroop Mishra, Tanglin Xia, Liang Qiu, Kai-Wei Chang, Song-Chun Zhu, Oyvind Tafjord, Peter Clark, and Ashwin Kalyan. Learn to explain: Multimodal reasoning via thought chains for science question answering. *NeurIPS*, 35: 2507–2521, 2022. 6, 13
- [59] Gen Luo, Yiyi Zhou, Yuxin Zhang, Xiawu Zheng, Xiaoshuai Sun, and Rongrong Ji. Feast your eyes: Mixture-of-resolution adaptation for multimodal large language models. *arXiv preprint arXiv:2403.03003*, 2024. 2
- [60] Ahmed Masry, Xuan Long Do, Jia Qing Tan, Shafiq Joty, and Enamul Hoque. Chartqa: A benchmark for question answering about charts with visual and logical reasoning. In *ACL*, pages 2263–2279, 2022. 6, 7, 13, 18
- [61] Minesh Mathew, Dimosthenis Karatzas, and CV Jawahar. Docvqa: A dataset for vqa on document images. In *WACV*, pages 2200–2209, 2021. 6, 7
- [62] Minesh Mathew, Viraj Bagal, Rubèn Tito, Dimosthenis Karatzas, Ernest Valveny, and CV Jawahar. Infographicvqa. In *WACV*, pages 1697–1706, 2022. 6, 7, 13, 17
- [63] Nitesh Methani, Pritha Ganguly, Mitesh M Khapra, and Pratyush Kumar. Plotqa: Reasoning over scientific plots. In *WACV*, pages 1527–1536, 2020. 13
- [64] Anand Mishra, Shashank Shekhar, Ajeet Kumar Singh, and Anirban Chakraborty. Ocr-vqa: Visual question answering by reading text in images. In *ICDAR*, pages 947–952, 2019. 13
- [65] Maxime Oquab, Timothée Darcet, Theo Moutakanni, Huy V. Vo, Marc Szafranec, Vasil Khalidov, Pierre Fernandez, Daniel Haziza, Francisco Massa, Alaaeldin El-Nouby, Russell Howes, Po-Yao Huang, Hu Xu, Vasu Sharma, Shang-Wen Li, Wojciech Galuba, Mike Rabbat, Mido Assran, Nicolas Ballas, Gabriel Synnaeve, Ishan Misra, Herve Jegou, Julien Mairal, Patrick Labatut, Armand Joulin, and Piotr Bojanowski. DINOv2: Learning robust visual features without supervision, 2023. 2
- [66] Alec Radford, Jong Wook Kim, Chris Hallacy, Aditya Ramesh, Gabriel Goh, Sandhini Agarwal, Girish Sastry, Amanda Askell, Pamela Mishkin, Jack Clark, et al. Learning transferable visual models from natural language supervision. In *International conference on machine learning*, pages 8748–8763. PMLR, 2021. 2, 5
- [67] Mike Ranzinger, Greg Heinrich, Jan Kautz, and Pavlo Molchanov. Am-radio: Agglomerative model – reduce all domains into one. 2023. 2
- [68] Chenglei Si, Yanzhe Zhang, Zhengyuan Yang, Ruibo Liu, and Diyi Yang. Design2code: How far are we from automating front-end engineering?, 2024. 19
- [69] Amanpreet Singh, Vivek Natarajan, Meet Shah, Yu Jiang, Xinlei Chen, Dhruv Batra, Devi Parikh, and Marcus Rohrbach. Towards vqa models that can read. In *CVPR*, pages 8317–8326, 2019. 6
- [70] Jianlin Su, Murtadha Ahmed, Yu Lu, Shengfeng Pan, Wen Bo, and Yunfeng Liu. Roformer: Enhanced transformer with rotary position embedding. *Neurocomputing*, 568:127063, 2024. 13
- [71] Quan Sun, Yuxin Fang, Ledell Wu, Xinlong Wang, and Yue Cao. Eva-clip: Improved training techniques for clip at scale. *arXiv preprint arXiv:2303.15389*, 2023. 13
- [72] S Svetlichnaya. Deepform: Understand structured documents at scale, 2020. 13
- [73] Peter Tong, Ellis Brown, Penghao Wu, Sanghyun Woo, Adithya Jairam Vedagiri IYER, Sai Charitha Akula, Shusheng Yang, Jihan Yang, Manoj Middepogu, Ziteng Wang, et al. Cambrian-1: A fully open, vision-centric exploration of multimodal llms. *Advances in Neural Information Processing Systems*, 37:87310–87356, 2024. 6, 13
- [74] Hugo Touvron, Thibaut Lavril, Gautier Izacard, Xavier Martinet, Marie-Anne Lachaux, Timothée Lacroix, Baptiste Rozière, Naman Goyal, Eric Hambro, Faisal Azhar, et al. Llama: Open and efficient foundation language models. *arXiv preprint arXiv:2302.13971*, 2023. 2
- [75] Penghao Wu and Saining Xie. V*: Guided visual search as a core mechanism in multimodal llms. In *Proceedings of the IEEE/CVF Conference on Computer Vision and Pattern Recognition*, pages 13084–13094, 2024. 18
- [76] Zhangchen Xu, Fengqing Jiang, Luyao Niu, Yuntian Deng, Radha Poovendran, Yejin Choi, and Bill Yuchen Lin. Magpie: Alignment data synthesis from scratch by prompting aligned llms with nothing. *arXiv preprint arXiv:2406.08464*, 2024. 13
- [77] Zhenhua Xu, Yujia Zhang, Enze Xie, Zhen Zhao, Yong Guo, Kwan-Yee K Wong, Zhenguo Li, and Hengshuang Zhao. Drivegpt4: Interpretable end-to-end autonomous driving via large language model. *IEEE Robotics and Automation Letters*, 2024. 2
- [78] Linli Yao, Lei Li, Shuhuai Ren, Lean Wang, Yuanxin Liu, Xu Sun, and Lu Hou. Deco: Decoupling token compression from semantic abstraction in multimodal large language models. *arXiv preprint arXiv:2405.20985*, 2024. 2
- [79] Jiabo Ye, Haiyang Xu, Haowei Liu, Anwen Hu, Ming Yan, Qi Qian, Ji Zhang, Fei Huang, and Jingren Zhou. mplug-owl3: Towards long image-sequence understanding in multi-

- modal large language models. In *The Thirteenth International Conference on Learning Representations*. 6
- [80] Jiabo Ye, Anwen Hu, Haiyang Xu, Qinghao Ye, Ming Yan, Guohai Xu, Chenliang Li, Junfeng Tian, Qi Qian, Ji Zhang, et al. Ureader: Universal ocr-free visually-situated language understanding with multimodal large language model. *arXiv preprint arXiv:2310.05126*, 2023. 6, 13
- [81] Weihao Yu, Zhengyuan Yang, Linjie Li, Jianfeng Wang, Kevin Lin, Zicheng Liu, Xinchao Wang, and Lijuan Wang. Mm-vet: Evaluating large multimodal models for integrated capabilities. In *International conference on machine learning*. PMLR, 2024. 6
- [82] Hang Zhang, Xin Li, Lidong Bing, and at al. Video-llama: An instruction-tuned audio-visual language model for video understanding. *arXiv preprint arXiv:2306.02858*, 2023. 2
- [83] Pan Zhang, Xiaoyi Dong Bin Wang, Yuhang Cao, Chao Xu, Linke Ouyang, Zhiyuan Zhao, Shuangrui Ding, Songyang Zhang, Haodong Duan, Hang Yan, et al. Internlm-xcomposer: A vision-language large model for advanced text-image comprehension and composition. *arXiv preprint arXiv:2309.15112*, 2023. 2, 7
- [84] Deyao Zhu, Jun Chen, Xiaoqian Shen, Xiang Li, and Mohamed Elhoseiny. Minigt-4: Enhancing vision-language understanding with advanced large language models. In *ICLR*, 2024. 1, 2
- [85] Fengbin Zhu, Wenqiang Lei, Fuli Feng, Chao Wang, Haozhou Zhang, and Tat-Seng Chua. Towards complex document understanding by discrete reasoning. In *Proceedings of the 30th ACM International Conference on Multimedia*, pages 4857–4866, 2022. 13

Appendix

A. Implementation Details

Training datasets. Table 7 shows the detailed dataset construction of the capability enhancement stage of HiRes-LLaVA. Specifically, it has 830K captioning including the ShareGPT4V [10], ShareGPT4o [32] and ALLAVA [7]. There are 821K OCR data from SynthDoG [30] including English OCR data as well as MMC-Alignment [49], UReader [80], K12 printed [1] which is a short OCR dataset. There is also 200K text instruction data from Magpie Pro [76], sampling from the data generated by Llama3.1-70B, Llama3-70B, and Qwen2-72B.

Task	Datasets(# Sample)	Sum
Caption	ShareGPT4V(89k), ALLAVA4V(684k), ShareGPT-4O(57k).	830K(44.8%)
OCR	SynthDoG-EN(300k), MMC-Alignment(200k), UReader(101k), K12 printed(120k), SynthDoG-ZH(100k).	821k(44.4%)
Text	Magpie Pro(200k)	200k(10.8%)
Total		1.8M

Table 7. Datasets in the capability enhancement stage.

Table 8 shows the detailed construction of the 3M instruction tuning dataset. First, we remove 23K caption data and ShareGPT data from original LLaVA-158K [51] and include GPT4V/GPT4o-generated caption data, i.e., LAION-GPT4v [33], ShareGPT4V [10], ShareGPT4o [32] and ALLAVA instruction data [7]. To enhance the common knowledge of our model, we convert the visual spatial reasoning [47], AI2D [28], and Science QA [58] training set into the instruct-tuning data. To activate the understanding science, we collect data from ViQuAE [35], TextbookQA [29], IconQA [57] and sampled 50k data from the Cambrian’s Data Engine [73]. We also collect document-oriented data from diverse datasets, includes ChartQA [60], DVQA [27], PlotQA [63], OCRVQA [64], ST-VQA [5], DocVQA [16], InfoVQA [62], DeepForm [72], TAT-DQA [85], TableFact [11], LRV-Chart[48] and WebSRC [12]. We merge some datasets from Cauldron [34], including RAVEN, ROBUT-SQA, ROBUT-WTQ, HiTab, IAM, Rendered Text, ORAND-CAR-A, Visual7W, Chart2Text, AI2D, vistext, Diagram-image-to-text.

Module Design Details. The self-mining sampler consists of one cross-attention block with an output layer norm. The cross-attention block has a cross-attention layer and a FFN.

Both of them apply the residual shortcut. The cross-attention layer has two layer norm for the query and key/value, respectively. As for the SliceRestore Adapter, the parameters of the self-attention layer with the layer norm are initialized from the pretrained CLIP self-attention at the same depth. To provide the positional information between slices, we apply a 2D RoPE [70, 71] on the global fusion module.

Training pipeline. We list the hyperparameters for the three-stage training at Tab. 9.

Evaluation details. We utilize the open-source evaluation tools, lmms-eval [37], to align our evaluation method to LLaVA-NeXT [53].

Benchmark construction. In our EntityGrid-QA, the construction of multiple choices is a vital part of EntityGrid-QA. For different types of entities, we apply different augmentations to obtain the other three choices for each question. For text and decimal, we randomly delete, add, or change one letter or digit. The object figures are collected from the COCO dataset [45]. For both categories of icons and objects, we use GPT-4 to list three other entities’ names with similar appearance as the negative options.

B. More Ablation

Comparison on the Same Training Set To demonstrate the effectiveness of our method, we compare the performance of LLaVA-1.5 and our method trained on the same data. Specifically, we train these two models on two different scale training data set, i.e., LLaVA-655K [38] and LLaVA-655K with additional Doc-79K data (the dataset of our ablation setting). Results from Tab. 10 show that adding 79K document data can highly improve models’ performance on ChartQA, DocQA and InfoVQA but slightly drops the performance on MMBench and MME-Perception. HiRes-LLaVA outperforms the LLaVA-1.5 under these two training data sets, confirms that the superior performance can be attributed to the method itself rather than the volume of data.

Ablation of the separators To further evaluate the effect of the separators, we conduct experiments on whether the separators are different or the same. Tab. 11 demonstrates that using separated separators greatly outperforms using the same ones which would confuse the model about the position of slices.

C. Efficiency Analysis

Comparison with other LVLMS. To validate the efficiency of our method, we compare the computational cost, training, and inference times with various LVLMS in Sec. C. For computational cost, we report the FLOPs of the ViT backbone, connector, and LLM components for each model. Experimental results demonstrate that HiRes-LLaVA, despite processing inputs at twice the resolution of LLaVA-Next (1344^2 vs. 672^2), is able to reduce training time by approximately

Task	Datasets(# Sample)	Sum
General QA	LLaVA(135K), ALLaVA(660K) VQAv2(83K), GQA(72K), OKVQA(9K), A-OKVQA(66K), VSR(12K), ShareGPT4V(89K), TextCaps(22K), Laion-GPT4V(11K), ShareGPT-4O(57K), RAVEN(3K), Visual7w(14K), RefCOCO(48K), VG(86K)	1.4M (48.0%)
Science	ScienceQA(19K), ai2d(14K), ViQuAE(4K), TextbookQA(21K), IconQA(30K), Data Engine(50K)	139K(4.6%)
Doc QA/OCR	OCRvQA(80K), TextVQA(57K), SynthDog(30K), LLaVAR(39K), WikiTableQuestions(29K), KleisterCharity(15K), iiii(6K), MLHME(30K), VisualMRC(19K), ChartQA(48K), DocVQA(102K), InfoVQA(33K), DVQA(200K), PlotQA(10K), TAT-DQA(2K), TableFact(65K), WebSRC(5K) DeepForm(8K), Chart2text(27K) Vistext(10K), chrome writing(9K), IAM(6K), Rendered text (10K), Orand-CAR-A(2K), lrv-chart(2K), ROBUS-SQA(9K), ROBUS-WTQ(4K), Hitab(3K), Diagram-image-to-text(0.3K).	0.9M(30.1%)
Code Generation	WebSight(50K)	50K(1.7%)
Text-only	Magpie-Pro(150K), Evol(142K), mathinstruct(81K), mathplus(95K).	469K(15.6%)
Total		3M

Table 8. Summary of datasets used in the instruction tuning stage.

	Settings	Stage-1	Stage-2	Stage-3
<i>Vision</i>	Resolution	$448 \times \{1 \times 2, \dots, 3 \times 3\}$	$448 \times \{1 \times 2, \dots, 3 \times 3\}$	$448 \times \{1 \times 2, \dots, 3 \times 3\}$
	# Tokens	Max $256 \times (1 + 9)$	Max $256 \times (1 + 9)$	Max $256 \times (1 + 9)$
<i>Data</i>	Dataset	LLaVA-Pretrain	Enhancement (Tab. 7)	SFT (Tab. 8)
	# Samples	558K	1.8M	3M
<i>Training</i>	Trainable	Projector	ViT & Projector & LLM	SRA & Projector & LLM
	Load SRA	\times	\times	\checkmark
	Batch Size	256	256	256
	LR: LLM	2×10^{-5}	2×10^{-5}	2×10^{-5}
	LR: Projector	1×10^{-3}	2×10^{-5}	2×10^{-5}
	LR: ViT / SRA	-	2×10^{-6}	2×10^{-4}
	Epoch	1	1	1

Table 9. **Detailed configuration for three-stage training of HiRes-LLaVA.** The table illustrates the vision configurations, dataset characteristics, and training hyperparameters.

Model	Data	VQA-Text	ChartQA	DocQA	InfoVQA	MMB	MME-P
LLaVA-1.5	LLaVA-665k	53.3	13.7	14.2	19.4	71.1	1459.66
LLaVA-1.5	LLaVA-665k + Doc-79k	53.3	23.8	22.6	31.4	70.7	1424.6
HiRes-LLaVA	LLaVA-665k	62.4	19.8	37.7	26.0	72.3	1486.1
HiRes-LLaVA	LLaVA-665k + Doc-79k	62.3	57.6	58.5	39.2	71.1	1444.8

Table 10. Ablation study of different training data. Using the same training data, our HiRes-LLaVA consistently outperforms LLaVA-1.5, demonstrating the superior effectiveness of our approach.

Type	VQA-Text	ChartQA	DocQA	InfoVQA	MMB	MME-P
Same	57.2	39.7	52.6	37.6	61.3	1379.8
Separated	61.8	58.8	59.7	41.4	65.5	1456.1

Table 11. Ablation of the separator. ‘Separated’ means three separators are the difference and ‘Same’ means that three separators are the same.

Training batch size	Inference Resolution	FLOPs			Training time	Inference time
		ViT	Connector	LLM		
<i>HiRes-LLaVA</i>						
2	1344x1344	6.6 T	195.2 G	37.1 T	60.7h (15.9%)	15.4m
<i>HiRes-LLaVA w/o SRA</i>						
2	1344x1344	6.5 T	195.2 G	37.1 T	59.5h (15.6%)	12.9m
<i>LLaVA-Next (LLaVA-1.6)</i>						
2	1344x1344	Out of the memory				
1	672x672	1.9 T	120.8 G	44.0 T	381.0h	13.2m

Table 12. Comparison of the efficiency of different models. Note that training time is assessed under the SFT setting on a machine with 8 V100 GPUs. The inference time is assessed on the InfoVQA benchmark with 6096 images by using the lmms-eval. Note that using the same batch size per device and resolution, LLaVA-Next would be out of the memory. The ratios of training time for ours relative to LLaVA-Next are marked in **purple**.

74%.

Comparison with other downsampling methods. We also compare the FLOPs and training time of our proposed downsampling strategy SMS with other vision token downsamplers, including ConcatChannel [8], Q-Former [3], and C-Abstractor [6], as shown in Tab. 13. The results show that our SMS, even when combined with additional components like SRA, achieves competitive efficiency compared to existing state-of-the-art downsamplers.

D. Discussion

What’s the goal of the EntityGrid-QA benchmark? The goal of our EntityGrid-QA benchmark is to assess the fragmentation issue in LVLMS (Large Vision-Language Models) when processing high-resolution inputs, rather than their ability to identify different types of objects. To address this, EntityGrid-QA synthesizes images by iteratively placing objects in different positions, allowing us to evaluate how these models perform on the edges and the center of the slices.

Components		FLOPs			Training Time
Downsampler	SRA	ViT	Sampler	LLM	
NoDownsample	×	6.5 T	410.8 G	148.3T	-
ConcatChannel	×	6.5 T	164.3 G	37.1 T	58.6h
Q-Former	×	6.5 T	205.5 G	37.1 T	58.9h
C-Abstractor	×	6.5 T	258.2 G	37.1 T	60.7h
SMS	×	6.5 T	195.2 G	37.1 T	59.5h
SMS	✓	6.6 T	195.2 G	37.1 T	60.7h

Table 13. Ablation study of the efficiency of individual components for different downsamplers. We assume the inputs are an image with 16 slices and 100 text tokens. Note that no downsampling method causes out-of-memory (OOM) issues during training. Training time is assessed under the SFT setting on a machine with 8 V100 GPUs.

Benchmarks	Slicing Strategy	Target Issue
LLaVA-UHD’s	Overlapped	Counting
Our EntityGrid-QA	Non-overlapped	Fragmentation

Table 14. The differences between our EntityGrid-QA and LLaVA-UHD’s benchmark [23].

Compared to harvesting real-world images with answer targets on the edges of slices, the synthesized approach is more simple-to-collect, effective, flexible, sufficient to evaluate the fragmentation issue.

Compared with LLaVA-UHD. The target issues and slicing strategies are different between Hires-LLaVA and LLaVA-UHD [23]. While LLaVA-UHD reveals the counting problem in the overlap slicing strategy for the high-resolution image inputs, Hires-LLaVA focuses on the fragmentation issues of non-overlapped slicing strategy which is commonly used in recent open-sourced high-resolution LVLMS. Table 14 summarize the differences of our EntityGrid-QA and LLaVA-UHD’s benchmark.

E. More Visualization

Samples from EntityGrid-QA Benchmark. We illustrate three examples from our proposed EntityGrid-QA benchmark in Fig. 6. These four samples visualize examples of the four tasks in the benchmark we proposed. For each task, we write or paste the digital number or object directly onto each position of an empty image, and ask questions to the models.

More Qualitative Results. To further validate the effectiveness of our model, we illustrate the more qualitative results of InfoVQA, ChartQA and V* Benchmark in Fig. 7 and Fig. 8. Moreover, we give two qualitative examples to present the HiRes-LLaVA’s capability of generating HTML code when given a website image in Fig. 9.

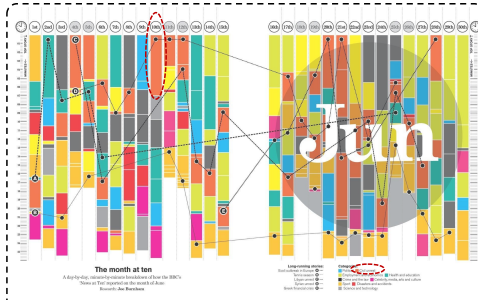


Figure 6. Examples of our proposed EntityGrid-QA Benchmark.

F. Broader Impacts

The development of HiRes-LLaVA advances the field of vision-language models and has broad implications for various applications, including document analysis, medical imaging and remote sensing. However, alongside these potential benefits, there are considerable concerns.

HiRes-LLaVA, not having undergone rigorous safety training, might generate harmful or inappropriate content, leading to legal and ethical issues. Furthermore, its enhanced ability to process high-resolution inputs could be misused for creating misleading news, contributing to disinformation. These potential negative impacts highlight the need for careful management and ethical guidelines in the deployment of such technologies.



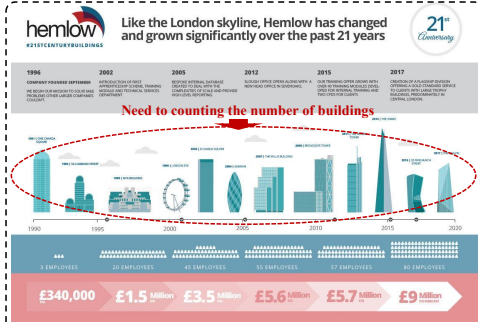
Q: What category was the *top story* on the 10th of June?

LLaVA-Next: politics \times Monkey: politics \times
Ours: civil unrest \checkmark



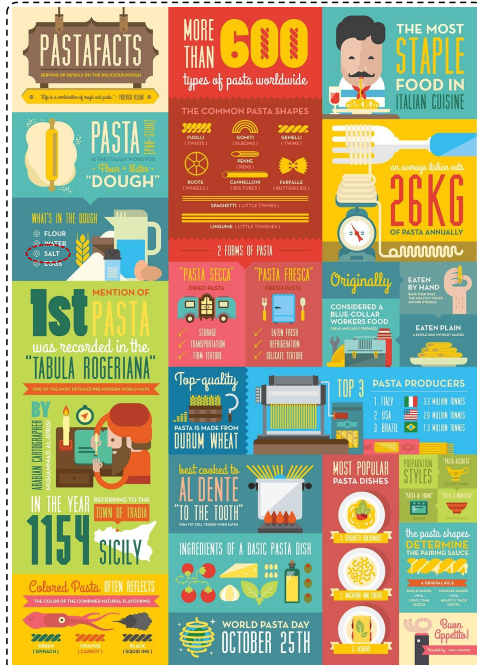
Q: Which environment issue is mentioned in the bottom row of the bulb image in the infographic?

LLaVA-Next: waste \times Monkey: pollution \times
Ours: ocean pollution \checkmark



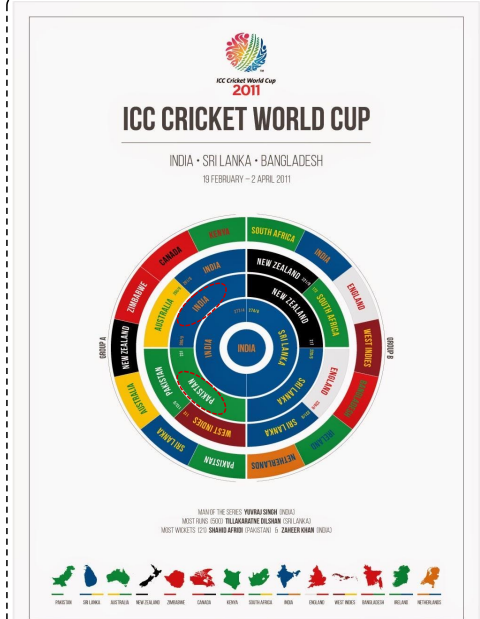
Q: How many buildings were constructed by Hemlow?

LLaVA-Next: 21 \times Monkey: 9 \times
Ours: 12 \checkmark



Q: What is the *third ingredient* listed to make Pasta?

LLaVA-Next: water \times Monkey: eggs \times
Ours: salt \checkmark



Q: Who was the *opponent of India* in the semifinals of World Cup 2011?

LLaVA-Next: england \times Monkey: sri lanka \times
Ours: pakistan \checkmark

Figure 7. Qualitative results from InfoVQA [62].

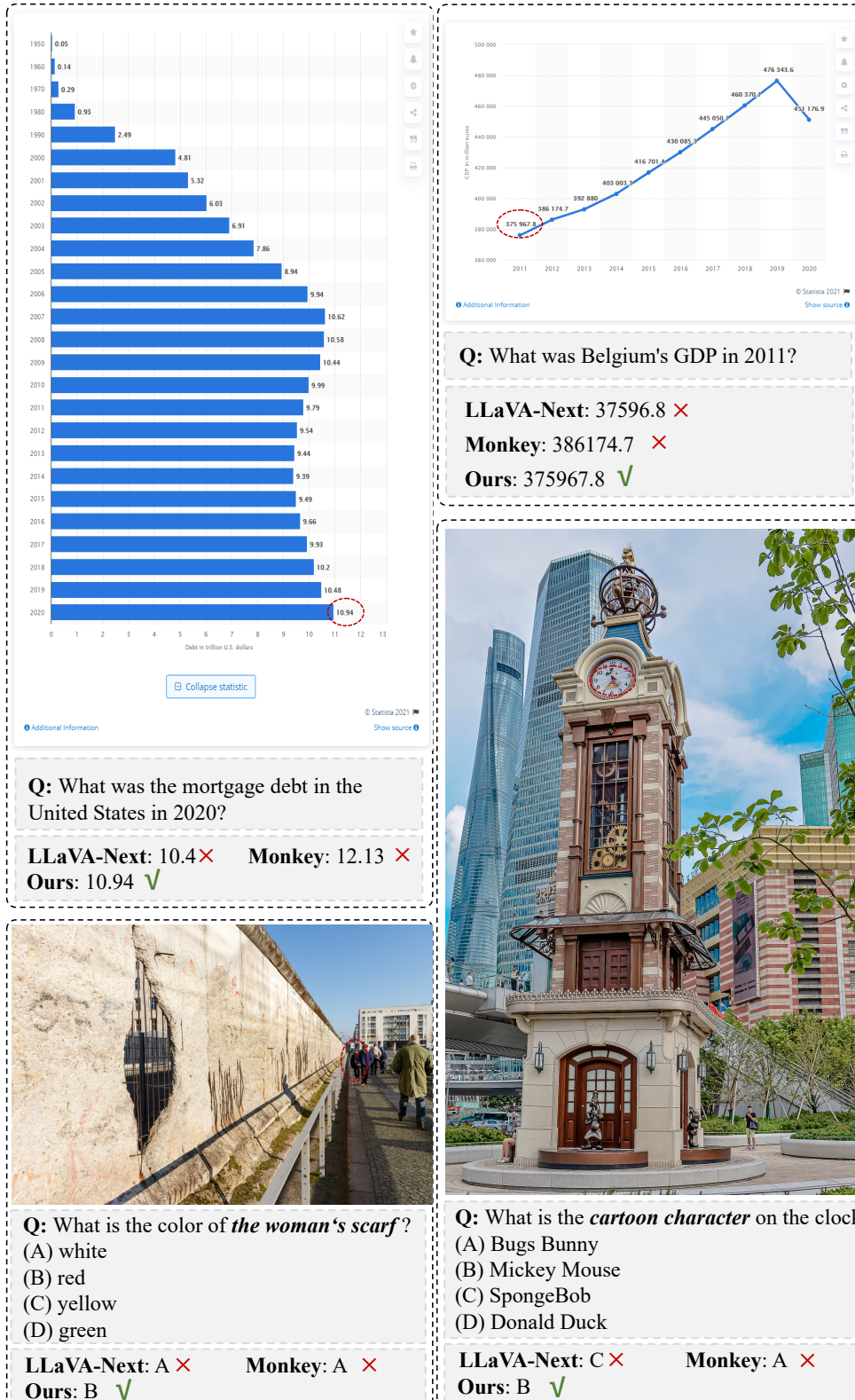


Figure 8. Qualitative results from ChartQA [60] and Vstar Benchmark [75]. We use the red circle to highlight the answer target in the image.

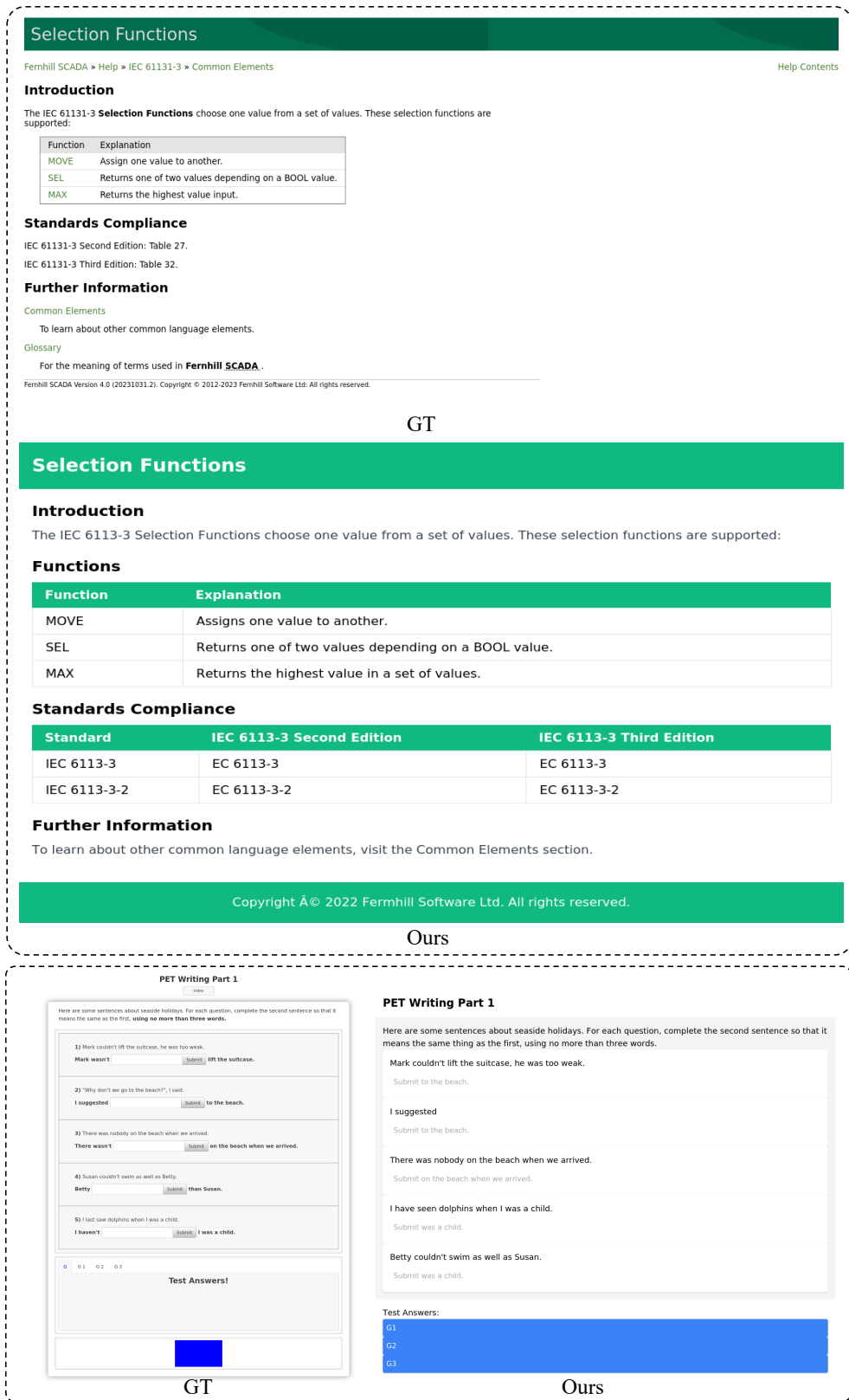


Figure 9. Qualitative results on Image2HTML task [68]. We visualize convert the generated html code to website image and compare to the input image.